Journal of Applied Fluid Mechanics, Vol. 18, No. 3, pp. 698-709, 2025.
Available online at www.jafmonline.net, ISSN 1735-3572, EISSN 1735-3645.
https://doi.org/10.47176/jafm.18.3.2867

Effect of Microchannel Depth on Subcooled Flow Boiling Instability and Heat Transfer

N. Shah, A. Prajapati, H. B. Mehta and J. Banerjee†

Department of Mechanical Engineering, Sardar Vallabhbhai National Institute of Technology Surat, India

†*Corresponding Author Email: jbaner@med.svnit.ac.in*

ABSTRACT

Microchannel heat sinks (MCHS) are capable of removing exceptionally high heat fluxes through liquid-to-vapor phase transition, making them suitable for various applications, including the thermal management of high-power microelectronics. However, their commercial applicability is hindered by the flow boiling instability associated with chocking of the micro-passage as the vapor bubbles grow. The present study addresses the research gap in literature pertaining to the impact of microchannel depth on flow boiling instability in terms of amplitude of heated surface temperature and pressure drop oscillations, and their influence on heat transfer performance. Experiments are conducted using dielectric water boiling in multiple parallel microchannels with mass fluxes of 220 and 320 kg/m²s and wall heat fluxes ranging from 25 kW/m² to 338 kW/m². Two different MCHS, fabricated from oxygen-free copper substrate, were examined, each comprising 44 parallel microchannels with nominal depths of 500 µm and 1000 µm, and a consistent nominal width of 200 µm. Heat transfer coefficients were measured using an array of embedded T-type thermocouples on the substrate to measure temperature gradients. The findings reveal that increasing the microchannel depth results to a significant increase in the amplitude of wall temperature fluctuations under fixed wall heat flux conditions, which in turn diminishes heat transfer performance. Additionally, the study demonstrates a notable dependence of pressure drop on coolant flow and both microchannel sizes. This research provides new insights into optimizing MCHS design for enhanced thermal management, highlighting the critical role of microchannel depth in mitigating flow boiling instability and improving overall heat transfer efficiency.

Article History

Received May 22, 2024
Revised August 27, 2024
Accepted September 21, 2024
Available online January 1, 2025

Keywords:

Boiling heat transfer
Microchannel
Instability
Boiling curve
Channel depth

1. INTRODUCTION

Higher operational temperatures can detrimentally impact the functionality of electronic devices, especially those subjected to substantial thermal loads within confined spaces. Consequently, efficient heat dissipation emerges as a significant bottleneck hindering the rapid advancement of miniaturization and integration in microelectronic technology. Tuckerman and Pease (1981), presented the idea of boiling flow in micro-channel heat sink for the cooling of high-speed VLSI circuits, which spurred decades of research in this field. The research in flow boiling through microchannel has attracted significant attention owing to its potential thermal efficiency.

However, the generation of excessive vapor within confined passages increases the resistance to coolant flow and leads to flow boiling instability. This results in continuous fluctuation in surface temperature and pressure (Kandlikar, 2004). Numerous studies have investigated various aspects of flow boiling instability in micro passages (Li et al., 2023; Abdellatif et al., 2024; Gao et al., 2024), including pressure drop characteristics (Ramesh & Gedupudi, 2019; Feng et al., 2023), the effect of coolant thermophysical properties (Sun et al., 2024), visualization of distinct flow regimes (Mehta & Banerjee, 2014; Zhao et al., 2021; Feng et al., 2024; Kokate & Park, 2024;), and geometric modifications within these passages to enhance boiling stability and improve heat transfer (Raj et al., 2020; Halon et al., 2022; Priy et al., 2024; Shah et al., 2024). These collective efforts were aimed to demonstrate the heat transfer potential of boiling flow within microchannel heat sinks while addressing pertinent issues related to instability. Several researchers reported use of different aspect ratios and hydraulic diameters to analyze

NOMENCLATURE

V	voltage applied to the heat sources	k	thermal conductivity
I	*current applied to the heat sources*	C_p	Specific heat
q	input power	A_s	heat sink base area
q_{fluid}	heat supplied to fluid	A_w	wetted area of the microchannel
q_{loss}	heat loss to the surrounding	x	space index
T_w	wall temperature	d	microchannel depth
T_s	measurement surface temperature	w	microchannel width
T_{savg}	average surface temperature	L	length of microchannel
y	distance between sensor measurement and channel bottom wall	n	number of microchannels
h_{fg}	latent heat of vaporization	T_{sat}	saturation temperature
X_e	exit vapour quality	T_{in}	inlet temperature
$S_{(x^+)}$	signal data above the mean value	$S_{(x^-)}$	signal data below the mean value
σ^+	standard deviation above the mean value	N	Number of recorded signal data
σ^-	standard deviation below the mean value	G	mass flux density
Q_w	wall heat flux density	htc	heat transfer coefficient
Nu	Nusselt number	Re_SP	Reynolds number of single-phase flow
Pr	Prandtl number	f_{fd}	fanning friction factor for fully developed flow
f_{app}	fanning friction factor for developing flow		

the thermohydraulic performances in micro-scale cooling technology. Singh et al. (2008) conducted boiling flow pressure drop measurements in microchannels with low aspect ratios, varying from 0.27 to 0.81, while keeping the constant 142µm of hydraulic diameter constant. They observed require small pumping power at an aspect ratio of 1.56. However, they noted that the pressure drop exhibited weak dependence on mass flux. Jiang et al. (2001) conducted experiments using di-water in silicone made triangular hydraulic diameters of microchannels with 26, 53 micrometers. They noted that vapour expansion emerged at relatively small heat flux levels, indicating that evaporative liquid-vapor interface dominated the heat transfer mechanism across a broad spectrum of input powers. Markal et al. (2016) conducted experiments with different aspect ratio of MCHS from 0.37 to 5 and keeping the hydraulic diameter fixed at 0.1 mm. Their findings indicate that boiling initiates at relatively higher superheated temperatures for aspect ratios lower than 1.5. Saitoh et al. (2005) conducted flow boiling experimental research with refrigerant R-134a flowing through three evaporative tubes with diameters of 0.5, 3 and 1 millimeters, for the mass fluxes of 150, 200, 300 and 400 kg/m^{2}s. Their findings indicated that the localized heat transfer coefficient (HTC) augmented with higher coolant flow in large sized tubes, but in smaller tubes, it showed little to no change in response to variations in mass flux. Soupremanien et al. (2011) empirically explored how aspect ratios (AR = 0.143 and 0.43) affect flow boiling in microchannels. Their research indicated that microchannels with lower aspect ratios enhance heat transfer performance at small heat flow levels but display a contrasting behavior under high heat flow condition. Moreover, the study highlighted the potential for premature dry-out occurrences in microchannels with lower aspect ratios. Harirchian and Garimella (2008) conducted experiments using various microchannel widths are ranging from 0.1 mm to 5.8 mm, while maintaining a consistent microchannel depth of 0.4 mm. Their findings indicate that in microchannels with widths equal to or greater than 400 µm, and for the same wall heat flux conditions, both the boiling curve and heat transfer coefficients remain unaffected by changes in channel size. Additionally, within the nucleate boiling region, boiling curve and HTC remain mass flow independent for a given microchannel size but are influenced by mass flow when convective boiling becomes predominant.

The existing literature predominantly examines the impact of lower aspect ratios in microchannels. However, a notable gap exists in literature on systematic investigations depicting the effect of depth in microchannel at higher aspect ratios on heat transfer and boiling instability. The literature reports very few studies where the depth of microchannel is larger to width, and the effect of such configurations on the amplitude of pressure and wall temperature oscillation is still underexplored. In the present work, experimental investigations are reported to evaluate the thermal behavior and analyze the boiling flow instability in two high-aspect ratio MCHS. The MCHS used have 44 parallel copper microchannels with width of 200 µm, depths of 500 µm (aspect ratio=2.5) and 1000 µm (aspect ratio=5) respectively. Experiments are performed using dielectric water for flow boiling under varying mass flux and heat flux conditions. The inlet condition is maintained at 15°C subcooled.

2. EXPERIMENTS

2.1 Flow Loop and Experimental Procedure

Experimental apparatus employed to carry out this research is illustrated in Fig. 1. The major components include a degassing unit, pulsation dampener, reciprocating metering pump, glass tube rotameter, pre-heater to set subcooled temperature using PID controller, strainer valve, microchannel heat sink test section, air-

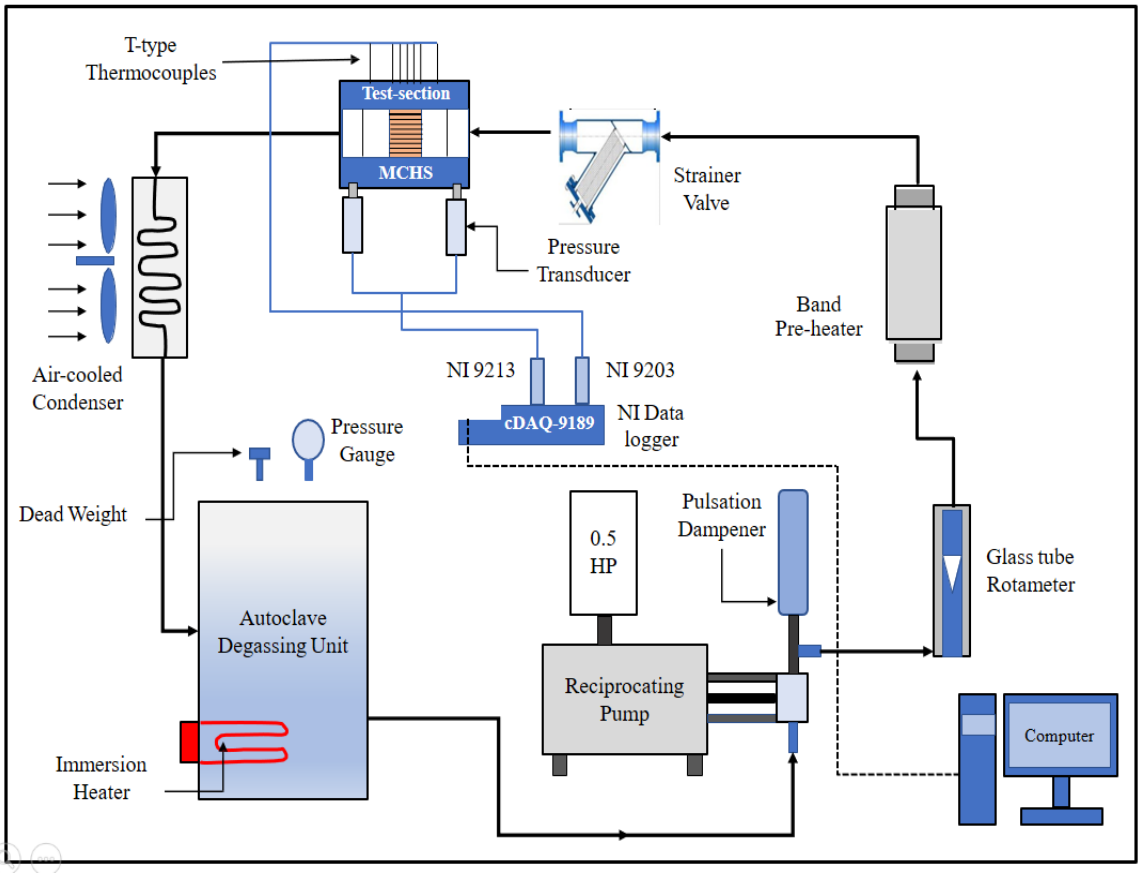

Fig. 1 Experimental flow loop

cooled finned copper tube heat exchanger, data acquisition system.

An Aluminum Autoclave Electric Immersion Heater Pressure Cooker (Capacity: 20 Liter) serves as working fluid reservoir. An immersion coil heater is utilized to degas the working fluid under high temperature and pressure conditions as per the procedure outlined in Chen and Garimella (2006). To minimize working fluid loss during degassing, a cooling system is positioned atop the degassing unit. The delivery of the required flow rate is achieved using a reciprocating positive displacement metering pump (Range: 0.36-9.6 LPH). A dampener is integrated to mitigate flow pulsations. Monitoring of the preset flow rate are facilitated by the Glass tube rotameter (Range: 0-18 LPH). Before entering the microchannel test section, the working fluid streams through a Y-type stainless steel filter valve fitted with a 0.04 mm Stainless steel mesh to filter out impurities. Temperature regulation at the inlet plenum of the MCHS is achieved using a PID controlled band-type preheater having 700-Watt maximum capacity. The desired subcooled temperature is set through this preheater. Heating of the Microchannel Test Section (MCHS) is facilitated by a DC variac controlling six cartridge heaters, each with a capacity of 200 Watts. Subsequent to passing through the test section, the working fluid undergoes a phase transition in the condenser from a two-phase flow to a liquid-phase flow before returning to the Autoclave chamber.

T-type thermocouples (accuracy ±0.25 °C) are utilized for monitoring the working fluid temperature at various points including the inlet-outlet plenum, as well as the substrate. These thermocouples are meticulously calibrated using liquid nitrogen's evaporation temperature, with saturated water temperature and ice cube temperature under atmospheric conditions. For assessing gauge pressure at both the inlet-outlet of the microchannel, a pair of WIka S-20 made gauge pressure transducers (with an absolute pressure range of 0-2.5 bar) are employed.

The pressure and temperature data are acquired using National Instrument-9203 data acquisition and monitored via LABVIEW. To protect the pressure transducer's diaphragm from potential damage due to elevated fluid temperatures, a cooling connector has been integrated. Crafted from aluminum, this cooling connector is designed with external fins to optimize heat dissipation, thereby reducing the temperature of the fluid reaching the pressure transducer.

2.2 Test Section

The MCHS test-section assembly is composed of oxygen free copper heating element, an heat resistance PTFE housing, and a polycarbonate sheet, as illustrated in Fig. 2. The MCHS are fabricated using vertical milling machine with forty-four parallel fins, each 200 μm thick and 20 mm in length. The experiments are reported here for two MCHS; one with 500 μm depth (aspect ratio =2.5) and other with 1000 μm depth (aspect ratio =5). The gap between two adjacent fins measures 200 μm. The PTFE housing accommodates the manifolds and the outlet-inlet plenums. Five T-type Copper-Constantan thermocouples are inserted just 2 mm below the microchannel heat sink

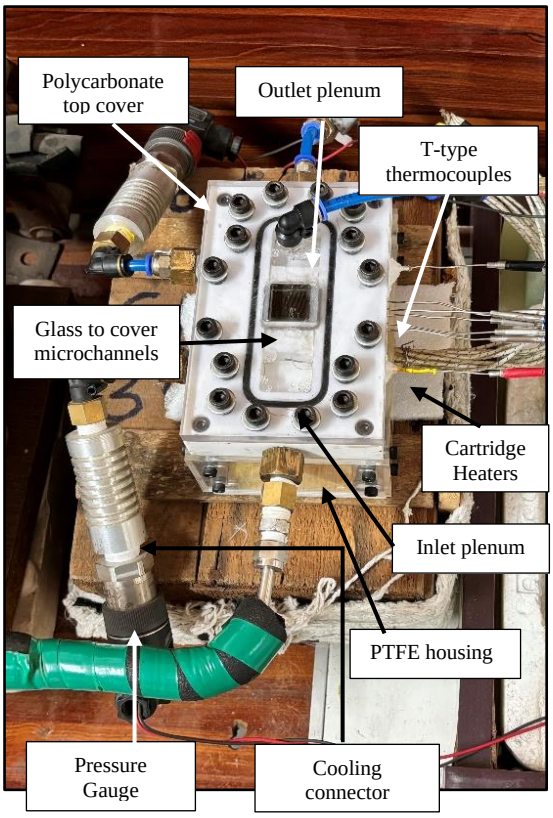

Photograph of Test Section

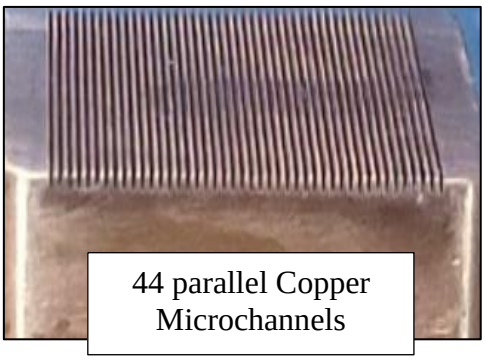

w= 200 µm, d = 500 µm

w= 200 µm, d = 1000 µm

Fig. 2 Microchannel test section

base. Working fluid temperature is measured at the entrance and exit of the microchannel.

3. DATA REDUCTION

The power delivered to the DC power cartridge heaters via an adjustable control panel is given by:

$$q = Voltage \times Current \tag{1}$$

where q represents the input power (Watt), determined from the voltage and current readings on the control panel. The heat removed by working fluid (q_{fluid}) is calculated as:

$$q_{fluid} = q - q_{loss} \tag{2}$$

Heat loss (q_{loss}) occurs through radiation and free convective heat transfer from the side wall surfaces to the surrounding environment, as well as from the top cover.

To reduce the heat losses, the heater section (heated copper element) is fixed in glass wool (thermal conductivity 0.037 W/mK) insulation within an acrylic box as shown in Fig. 2. This heat loss is established prior the MCHS is charged with working fluid. Under this condition, the temperature of each sensor is recorded when heaters are activated by constant power supply till it reaches steady state. A linear correlation $q_{loss} = 0.06 \times T_{savg} - 4$, is established between the heat loss (q_{loss}) and steady state average surface temperature (T_{savg}) by repeating this procedure for several levels of input power.

The local wall substrate temperature $T_{w,x}$ is determined from the local temperature measurement at the base of the MCHS substrate, $T_{s,x}$, using the following equation:

$$T_{w,x} = T_{s,x} - \frac{q_{fluid} \times \mathrm{z}}{k \times A_s} \tag{3}$$

Here, 'z' represents the distance from the MCHS Substrate to the thermocouple, $'A_s'$ is the MCHS base area, and *'k'* denotes the thermal conductivity of heating block.

To effectively compare the performance of microchannel, it is essential to assess the heat flux density. The wall heat flux density (Q_w) is determined in terms of heat transferred to the wetted area of coolant flow within the microchannel $\left(\frac{q_{fluid}}{A_w}\right)$. Here A_w is the wall wetted area of MCHS and is calculated as: $A_w = n(w + 2d) \times L$; where w is the width of the microchannel, n is the number of multiple microchannels, d is the depth of the microchannel and L is the length of the microchannel.

The vapor quality at exit of MCHS (x_e) is obtained from energy balance is as follows:

$$x_e = \frac{1}{h_{fg}}\left(\frac{q_{fluid}}{\dot{m}} - C_{p,f}(T_{sat} - T_{in}\right) \tag{4}$$

Heat transfer coefficient (htc) is calculated as:

$$htc = \frac{Q_w}{T_w - T_R} \quad (5)$$

T_R is the reference temperature. In subcooled flow boiling regime T_R is the fluid temperature (T_f) and in saturated flow boiling regime T_R is the saturated fluid temperature (T_{sat}). The experimental uncertainty in measurements of pressure drop, temperature and volume flow rate are ±0.003 bar (0.25% of full scale), ±0.25 °C and ± 2% respectively. Derived uncertainty for heat transfer input is ±2% and for heat dissipated it is ±1.82 %.

3.1 Experimental Validation

Single-phase validation test were conducted in the microchannel heat sink with aspect ratios (AR) of 2.5 and 5, over a Reynolds number range of 150 to 450, at a continual base heat flow and inlet subcooling (q_b= 117 kW/m^2 and T_{in} = 85 °C). The heat loss was calculated from the above-mentioned correlation which is depends upon the base temperature of MCHS. It is fount that, it is to be less than 7%, even at high wall temperatures.

Correlations from Shah and London (1978) are used to the obtain liquid-phase Nusselt number and pressure drop in microchannels and these are compared with our experimentally evaluated Nusselt Number in Fig. 3 (a).

$$Nu = 9.12305 + 0.0312 \times \frac{RePr^{0.4}}{AR}; \quad (6)$$

$$200 < Re < 1500, 0.5 < \Pr < 10^6$$

Fanning friction factor for fully developed flow:

$$f_{fd} = \frac{po}{Re},$$

$$po = 24 \times \left[1 - \frac{1.3553}{AR} + \frac{1.9467}{AR^2} - \frac{1.7012}{AR^3} + \frac{0.9564}{AR^4} - \frac{0.2537}{AR^5}\right] \quad (7)$$

For the AR=2.5, po=16.57, for the AR=5, po=19.169.

Fanning friction factor for developing flow:

$$f_{app} = \frac{1}{Re}\left[3.44\left(L_{sp}\right)^{-0.5} + \frac{0.125/(4L_{sp})f_{fd}Re - 3.44{L_{sp}}^{-0.5}}{1+1.31\times10^{-4}{L_{sp}}^{-2}}\right] \quad (8)$$

$$L_h = 0.05ReD_h;\ f_{sp} = f_{app}\ if\ L_{sp} < L_h;$$

$$f_{sp} = f_{app}\ if\ L_{sp} > L_h$$

$\Delta P_{ch} = \Delta P_{meas} - \Delta P_{loss}$, where ΔP_{ch} is channel pressure drop, ΔP_{meas} is pressure measured by transducer and pressure loss by inlet and outlet sudden contraction and sudden enlargement by ΔP_{loss}. $\Delta P_{loss} = \frac{1}{2}\rho\bar{V}_{ch}^2(K_c + K_e)$.

Abrupt contraction and enlargement at and inlet and outlet create and pressure loss and it is denoted as K_e and K_c, can be assessed using the methods outlined by Kays and London (1984), which depend on the ratio of the plenum to microchannel flow areas and the flow regime. The Fanning friction factor, calculated from the microchannel pressure drop (f_{meas}), is expressed as follows:

$$f_{meas} = \frac{\Delta P_{ch}}{2L\rho\bar{V}_{ch}^2} \quad (9)$$

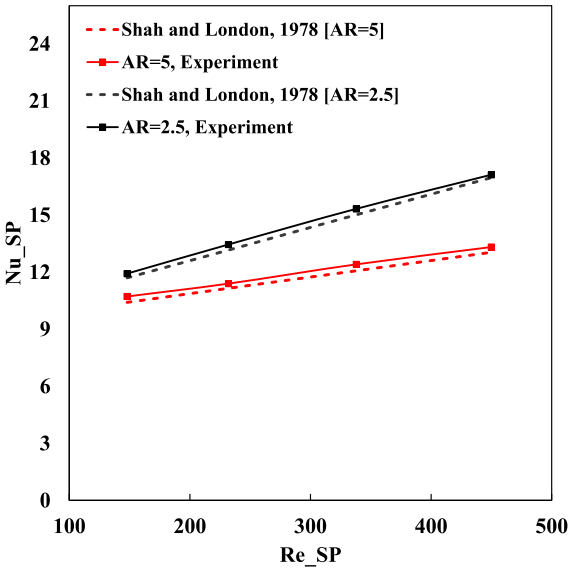

(a)

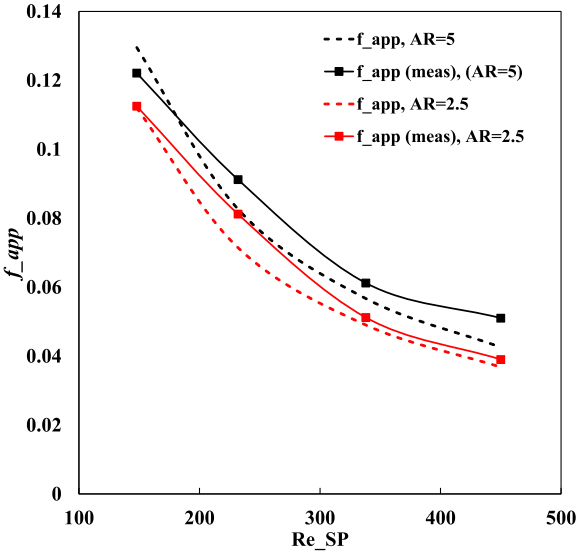

(b)

Fig. 3 Single phase validation. (a) Nu versus Re, (b) Friction factor versus Re

Where, $\bar{V}_{ch}$ is mean velocity of the channel (meter/seconds). L is the microchannel length (meter). ρ is the density (kg/m^3). These are compared with our experimentally evaluated friction factor in Fig. 3(b).

4. RESULTS AND DISCUSSION

The experiments are presented here for wall heat flux of 20-300 kW/m^2 and mass flux density of 220 and 320 kg/m^{2}s. The inlet fluid temperature is kept at 85°C (15°C subcooled). The heat transfer performance is first depicted here using the flow boiling curve estimated in terms of measured variation of substrate wall temperature.

Flow boiling instability is measured in terms of amplitude of fluctuations in pressure drop and substrate temperature. The standard deviation below and above the

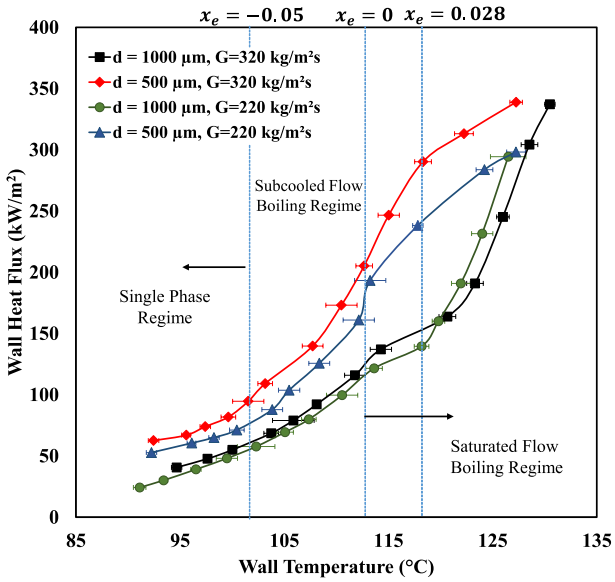

Fig. 4 Flow boiling curve

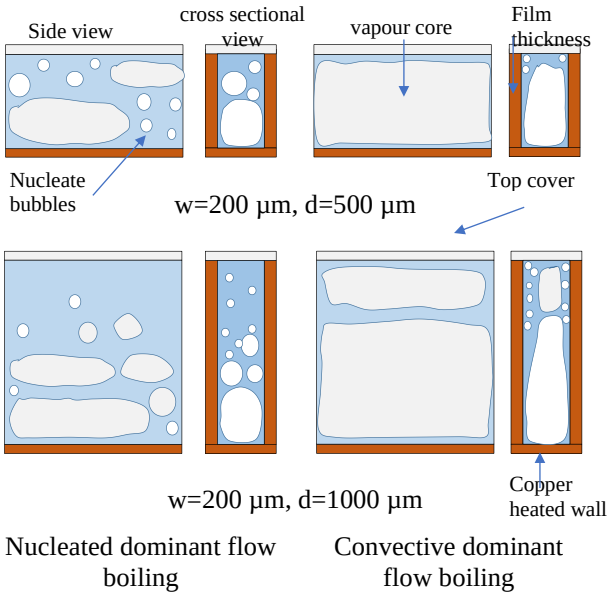

Fig. 5 Schematic view of vapour interface developed in swallow and deeper microchannel

mean value are computed as $\sigma^+ = \sqrt{\frac{\Sigma\left(S_{(x+)} - \bar{S}\right)^2}{N}}$, and $\sigma^- = \sqrt{\frac{\Sigma\left(S_{,(x^-)} - \bar{S}\right)^2}{N}}$, respectively. Here, S is recorded signal with time. The range between the standard deviation of pressure drop and surface temperature signals below the mean value (σ^-) and above the mean value (σ^+) is used as the amplitude of fluctuations.

4.1 Flow Boiling Curve

Figure 4 illustrates the flow boiling curve estimated based on the present experiments for both the microchannel of depth 500 µm and 1000 µm. The measured temporal averaged microchannel surface temperature is depicted in the boiling curve for changing heat fluxes and different values of mass fluxes. The curves encompass both boiling and single-phase regimes. The two-phase regimes include the subcooled boiling flow regime and the saturated boiling flow regimes.

As shown in Fig. 4, in the single-phase regime (30-100 kW/m²s), the increasing substrate temperature increases almost linearly with heat flow density. Moreover, increasing the mass flux leads to a delay in the onset of nucleate boiling (ONB). It is also observed that the ONB occurs at a higher heat flux in shallower microchannel (d=500 µm). After the ONB, an increase in wall heat flux leads to higher void fractions in flow boiling, resulting in a transition from liquid-phase to subcooled boiling flow.

The ONB was observed in all channels when the microchannel base wall temperature reached 2-3 degrees Celsius above the saturation temperature. Similar observations are also reported in (Liu et al., 2005; Hedau et al., 2022). However, while the temperature required for ONB is consistent across different channels, the heat fluxes required for achieving this base wall temperature vary depending on the mass fluxes and channel sizes.

Figure 3 shows, in the subcooled flow boiling, the MCHS substrate temperature rises slowly with increasing wall heat flux due to nucleate and bubbly flow regime. The thermal performance of shallower microchannel is better compared to deeper microchannel during the transition from single-phase to subcooled boiling flow, as depicted in the boiling curve (Fig. 4). The bulk outlet fluid temperature remains below saturation in the subcooled boiling flow condition. When the temporal averaged outlet fluid temperature reaches saturation, the exit vapor quality is calculated to be zero. Our experiments show that when the surface temperature reaches 112-114 °C with increasing heat flux, the exit vapor quality tends to zero for both microchannels, although the heat flux values differ. This indicates that the flow boiling curve depends on channel size.

Further increase in heat flux increasing the exit vapor quality, transitioning subcooled boiling flow to saturated boiling flow conditions, where the fluid temperature remains saturated as the heat flux increases. The transition from subcooled to saturated flow boiling decreases heat transfer performance in deeper microchannels when the vapor quality is lower than 0.028. In low vapor quality saturated flow boiling, the regime is dominated by nucleate and bubbly flow, as explained using schematic view of the vapor interface for both the microchannels in Fig. 5. As exit vapor quality increases in saturated flow boiling, boiling heat transfer is dominated by conventional flow boiling where liquid film thickness plays crucial role in heat transfer. As shown in Fig. 5 the area of liquid film thickness is increasing in deeper microchannel, thereby increasing the heat transfer efficiency.

The boiling flow curves are observed to be mass flow independent in the flow regime cycle (100-240 kW/m²s). However, under higher heat flux (above 240 kW/m²s) conditions, a rise in substrate temperature is observed at a low mass density of 220 kg/m²s. This is due to premature transition from slug to annular flow at low mass flux. Due

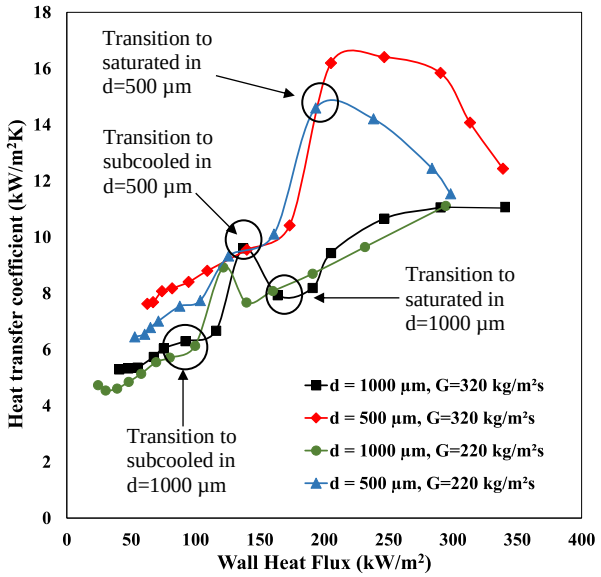

Fig. 6 Heat transfer coefficient

to insufficient mass flow inventory, the inlet momentum is inadequate to overcome the resistance developed by the annular regime thereby leading to excess surface temperature. This can lead to longer dryout period. This effect is more for shallower channel as can be observed from Fig. 4.

Initially, as boiling commences, the wall temperature shows a mild correlation with heat flux. However, as the wall heat flux rises, the wall temperature increases, resulting in noticeably distinct boiling curves between microchannels with depths of 500 µm and 1000 µm. For the same wall heat flux, deeper channel experienced higher wall temperature in comparison to the shallower one. This indicates poor heat transfer performance in deeper microchannel. This is attributed to the rapid increase in vapor quality and the early formation of annular flow within the microchannel with a shallower depth.

The coefficient of heat transfer is plotted against heat flux for both mass fluxes and microchannel sizes, as shown in Fig. 6. To calculate the heat transfer coefficient, different temperature references are used depending on the flow condition. In the subcooled regime, the difference of fluid and the wall substrate temperature is taken into account. Conversely, in the saturated flow condition, the excess wall temperature relative to the saturated fluid temperature is used. The transition regime with heat flux is identified from Fig. 4 and mentioned in Fig. 6. The small variation in the trend of surface temperature and heat flux causes a notable twist in the HTC, as it depends on the average fluid temperature and surface temperature. The randomness in the HTC also appears in literature (Wang & Sefiane, 2012; Wang et al., 2023). The data reveals an early transition in subcooled to saturated boiling flow in deeper microchannel. In the subcooled flow boiling regime, the coefficient of heat transfer increases for both microchannel sizes, with the shallower microchannel exhibiting a higher magnitude. Under the saturated flow, the coefficient of heat transfer is initially high during the nucleate boiling dominant phase but shows poor performance at higher heat fluxes for shallower microchannel.

4.2 Surface Temperature Fluctuations

The flow boiling instability in terms of surface temperature fluctuations are shown in Fig. 7 and 8. The transient variation of surface temperature at the medium heat flux level of 160 kW/m^2 shown in Fig. 7. This figure illustrates that the surface temperature fluctuations are nearly identical across varying mass fluxes. This is true for both the microchannel. However, the amplitude of surface temperature fluctuations is significantly influence by the channel depth. This is demonstrated in Fig. 8. A significant increase in the amplitude of average surface temperature fluctuations is observed for the case of the deeper microchannel (1000 µm) compared to the shallower one (500 µm).

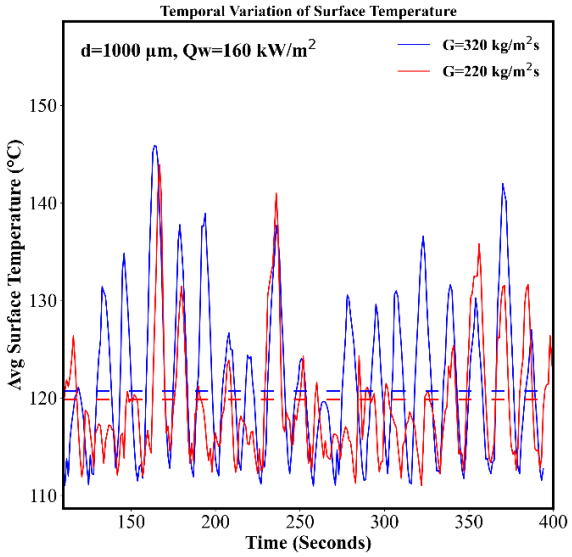

Fig. 7 Temporal variation in wall temperature, effect of mass flux

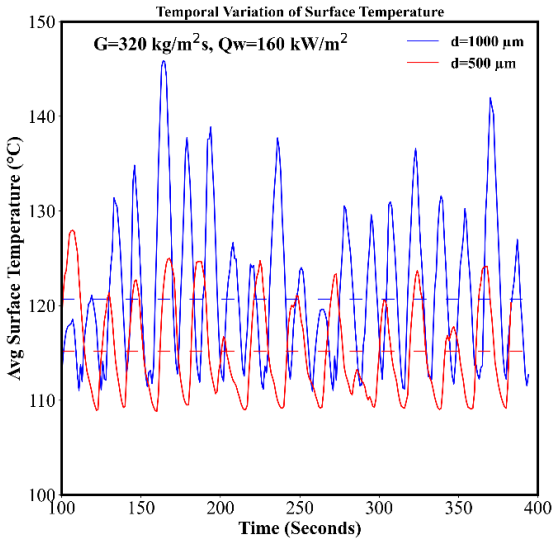

Fig. 8 Temporal variation in wall temperature, effect of channel depth

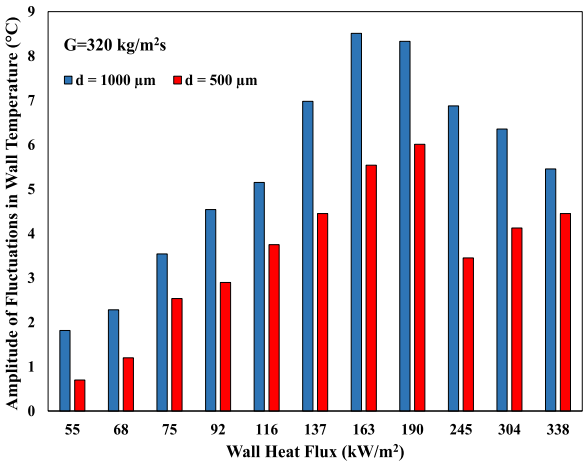

(a)

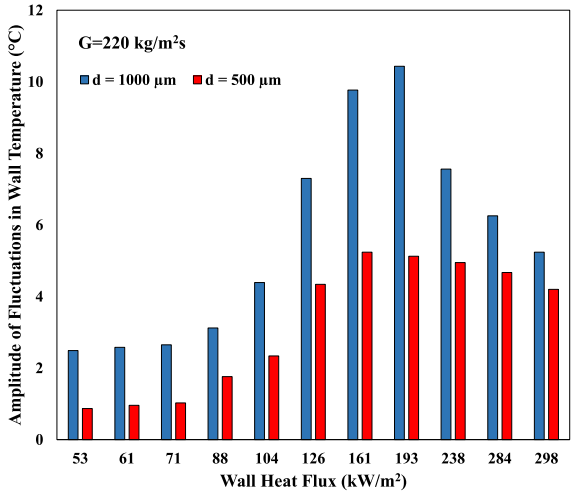

(b)

Fig. 9 Amplitude of fluctuations in substrate temperature

The impact of heat flux on the average amplitude of substrate temperature fluctuations in both microchannels is elucidated in Fig. 9 (a) and (b), corresponding to mass fluxes of 320 and 220 kg/m²s, respectively. Within the medium heat flux range of 70 kW/m² to 190 kW/m², surface temperature fluctuations escalate with rising heat flux due to cyclic variations in the flow regime within the microchannels. As vapour bubbles form within the heated micro passages, they swiftly expand, constricting the passage and causing the bubble interface to oscillate back and forth. This motion intermittently obstructs the passage, momentarily halting the influx of fresh coolant. Consequently, the mass flux declines. However, the pump continuously delivers fresh coolant, and once the pressure exerted by the coolant surpasses the backflow pressure, the microchannels are re-wetted by liquid coolant. This cyclic process repeats during medium heat flux conditions.

With increasing heat flow in this range, more vapor is generated, prolonging the duration of backflow and dryout conditions, ultimately resulting in heightened amplitude of fluctuations. Furthermore, the amplitude of these fluctuations is notably higher in the deeper MCHS compared to the shallower one in medium heat flux conditions. Under saturated flow boiling condition, stability is enhanced due to the pivotal role played by the evaporative film in the boiling flow process. Initially, the amplitude of oscillations decreases with wall heat flux and then starts to increase for shallower microchannel. However, in deeper microchannel, the difference in the amplitude of fluctuations as compared to shallower one is less under saturated flow conditions.

At a mass flux of 320 kg/m^{2}s, the average amplitude of oscillations in surface temperature, encompassing both liquid-phase and boiling conditions, measures 5.39°C in microchannels with a depth of 1000µm and 3.55°C in channels with a depth of 500µm. On the other hand, at a mass flux of 220 kg/m^{2}s, the corresponding amplitudes are 5.61°C in 1000µm channel depth and 3.22°C in 500µm channel depth.

The amplitude of heat flow density fluctuations typically decreases as the flow boiling approaches saturation. However, in shallower microchannels at lower mass fluxes (G = 320 kg/m²s) and higher heat fluxes (>300 kW/m^2), the increased vapor generation may lead to more frequent blockages of the microchannel passages. In deeper microchannels, non-uniform wall temperatures, especially with fins, cause vapor bubbles to concentrate primarily at the bottom sections. The greater available space in deeper channels reduces the likelihood of microchannel blockages. Therefore, despite the higher heat flux, the amplitude of heat flow density fluctuations can increase at G = 320 kg/m²s and a depth of 500µm due to these localized vapor generation and channel blockage dynamics.

4.3 Instability in Pressure Drop

The variations in pressure drops within the microchannel are shown in Fig. 10, demonstrating their connection to the average wall heat flux. A notable distinction between the single-phase and boiling flow regimes is apparent, marked by a change in the slopes of the curves. In the single-phase regime, the pressure drop exhibits a slight decrease as the heat flux increases, attributed to the reduction in liquid viscosity with rising temperature. In contrast, within the boiling flow region, the pressure drop is strongly influenced by the heat flux, increasing rapidly and almost linearly. This is due to vapor acceleration and the associated frictional pressure drop in the boiling flow. At low mass fluxes (220 kg/m^{2}s), early achievement of saturated flow boiling results in lower in pressure drop at higher heat flux conditions. These observations are consistent with findings reported in various studies (Harirchian and Garimella, 2008; Markal et al., 2016).

Figure 10 illustrates the effect of different microchannel sizes on pressure drop at a constant mass flow rate, demonstrating its variation with wall heat flux. Across both liquid-phase and boiling flow regions, reducing microchannel depth leads to an increase in pressure drop at a applied heat flux. Particularly in the two-phase domain, as the channel depth decreases, the slope of the pressure drop curve increases, resulting in

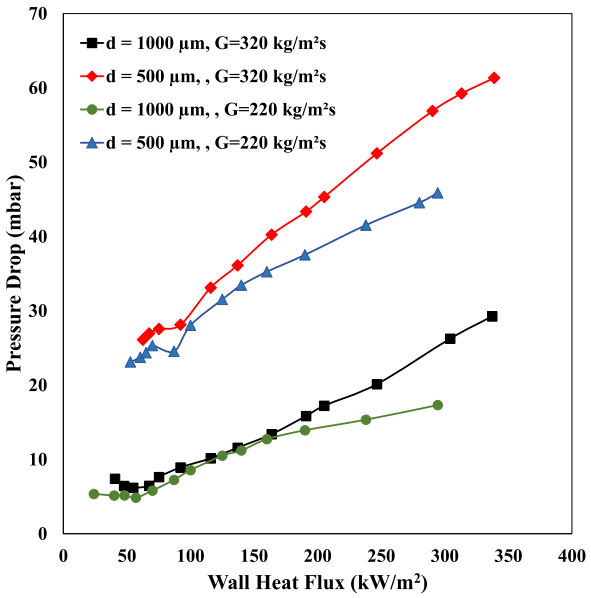

Fig. 10 Effect of mass flux and heat flux on pressure drop

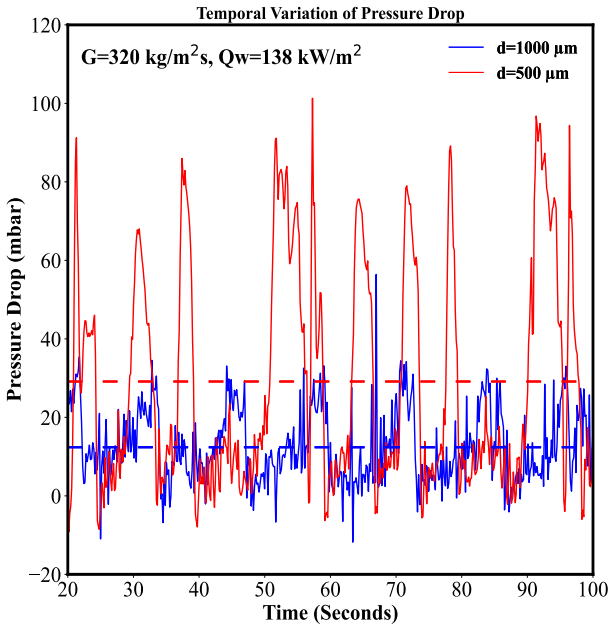

Fig. 12 Temporal variation in pressure drop

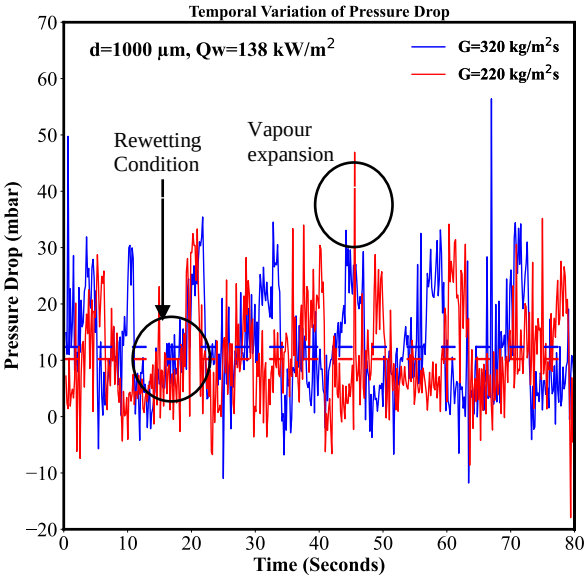

Fig. 11 Temporal variation in pressure drop

significantly higher pressure drops for shallower microchannel under higher heat flux conditions

Oscillations in pressure drop is presented in Fig. 11 for the both mass fluxes in deeper microchannel (depth 1000µm). These oscillations depict cyclic change in flow boiling regimes in heated micro passage during boiling. This leads to continuous change in flow. The crest in pressure signal shows the vapor expansion period and the low amplitude oscillations with high frequency indicates the rewetting phenomena. The amplitude of pressure drop oscillation is almost identical for both mass flux under the same wall heat flux conditions.

The impact of channel size on pressure drop oscillations is depicted in Fig. 12. It reveals that the amplitude of pressure drop oscillations is notably higher in shallower microchannel. This is because lower cross-sectional area leads to rapid accumulation of vapor bubbles that obstruct the micro-passage. In deeper microchannel, a larger available flow area mitigates this issue as discussed earlier in context to Fig. 5. The buoyancy force naturally drives vapor upwards, creating a passage for coolant flow beneath the vapor layer. Consequently, this reduces the pressure drop oscillations. However, frequency of cyclic oscillations is less in shallower microchannel compared to that observed in deeper microchannel. The high frequency with lower amplitude fluctuations indicate frequently rewetting.

The influence of heat flux on the amplitude of fluctuations in both microchannel, under mass flux conditions of 320 and 220 kg/m^{2}s, is depicted in Fig. 13 (a) and (b) respectively. At lower heat flux conditions, the onset of nucleation occurs earlier, leading to increased pressure drop fluctuations in deeper microchannel even at lower heat flux levels. It is evident that as the heat flux rises, so does the amplitude of oscillation in pressure drop, observed across both microchannel and heat flux values, until it reaches the saturated flow boiling regime. Within this regime, characterized by higher heat fluxes, the flow dynamics results in reduction of the magnitude of pressure drop oscillations.

The amplitude of pressure drop oscillations is show a contrasting behavior compared to what is depicted by surface temperature variation. At a mass flux of 320 kg/m^{2}s, the average amplitude of oscillations in pressure drop, encompassing both single-phase and boiling flow conditions, measures 10.12 mbar for the microchannel with depth of 1000µm and 19.1 mbar in channel with a depth of 500µm. Meanwhile, at a mass flux of 220 kg/m^{2}s, the corresponding amplitudes are 7.02 mbar for 1000µm channel depth and 10.5 mbar for 500µm channel depth.

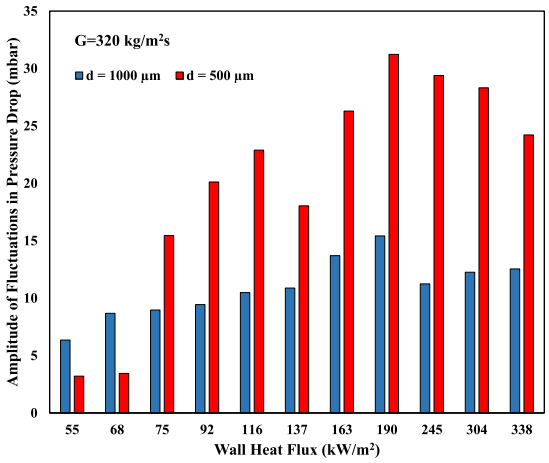

(a)

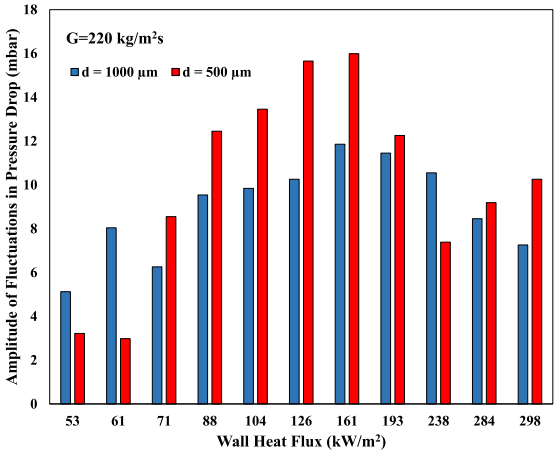

(b)

Fig. 13 Amplitude of pressure fluctuations

5. CONCLUSIONS

The effect of microchannel depth and mass flux on subcooled flow boiling instability and heat transfer is reported here for DI-water flow boiling through 44 parallel straight-through microchannel.

1. Analysis of the flow boiling curve derived from our experiments unveils a significant increase in surface temperature fluctuations within the subcooled flow boiling regime and a marginal rise within the saturated flow boiling regime, particularly evident in deeper microchannel. Consequently, the heat transfer efficiency of deeper microchannel is enhanced during saturated flow boiling, characterized by a vapor quality exceeding 0.028.
2. In the realm of subcooled flow boiling, we observe a notable enhancement in the HTC across both microchannel sizes. The shallower microchannel demonstrate a more pronounced increase in magnitude. Transitioning to the saturated flow regime, we find that the HTC initially peaks during the initial nucleate boiling phase and diminishes in convective boiling phase for shallower microchannel.
3. The pressure drop oscillations are higher in shallower microchannel owing to lower cross-sectional area of flow which leads to rapid accumulation of vapor bubbles that obstruct the micro-passage.
4. In deeper microchannel, owing to a larger available flow area, the buoyancy force naturally drives vapor upwards, creating a passage for coolant flow beneath the vapor layer. Consequently, this reduces the pressure drop oscillations. However, frequency of cyclic oscillations is higher in deeper microchannel.

ACKNOWLEDGEMENTS

The authors gratefully acknowledge the financial assistance provided by Gujarat Council on Science and Technology (GUJCOST), Gujarat, India (sanction letter no. GUJCOST/STI/R&D/23-24/1682) for this research.

CONFLICT OF INTEREST

The authors declare that there is no conflict of interest with any individual or organization as far as this research is concerned.

AUTHORS CONTRIBUTION

N. Shah: Conceptualization, Methodology, Software, Data Curation, Visualization, Writing – Original Draft; **A. Prajapati:** Literature, Analysis; **H. B. Mehta:** Methodology, Supervision, Interpretation of Results, Writing – Review & Editing, Project Administration; **J. Banerjee:** Conceptualization, Supervision, Critical Feedback, Interpretation of Results, Writing –Review & Editing, Principal Investigator.

REFERENCE

Abdellatif, H. H., Ambrosini, W., Arcilesi, D., Bhowmik, P. K., & Sabharwall, P. (2024). Flow instabilities in boiling channels and their suppression methodologies—A review. *Nuclear Engineering and Design, 421*, 113114. https://doi.org/10.1016/j.nucengdes.2024.113114

Chen, T., & Garimella, S. V. (2006). Effects of dissolved air on subcooled flow boiling of a dielectric coolant in a microchannel heat sink. https://doi.org/10.1115/1.2351905

Feng, L. L., Cao, C. C., Zhong, K., & Jia, H. W. (2023). Investigation of flow boiling in micro-channels: heat transfer, pressure drop and evaluation of existing correlations. *Journal of Applied Fluid Mechanics*, *16*(9), 1717-1728. https://doi.org/10.47176/jafm.16.09.1840

Feng, L., Zhong, K., Lei, Y., & Jia, H. (2024). Flow pattern-based heat transfer analysis of microchannel flow boiling: An experimental investigation. *Case Studies in Thermal Engineering*, *54*, 104016. https://doi.org/10.1016/j.csite.2024.104016

Gao, Y., Wang, Z., Li, Y., Ma, E., & Yu, H. (2024). Flow

boiling of liquid nitrogen in a horizontal macro-tube at low pressure: Part I-flow pattern, two-phase flow instability, and pressure drop. *International Journal of Heat and Fluid Flow*, *107*, 109335. https://doi.org/10.1016/j.ijheatfluidflow.2024.109351

Halon, S., Krolicki, Z., Revellin, R., & Zajaczkowski, B. (2022). Heat transfer characteristics of flow boiling in a micro channel array with various inlet geometries. *International Journal of Heat and Mass Transfer*, *187*, 122549. https://doi.org/10.1016/j.ijheatmasstransfer.2022.122549

Harirchian, T., & Garimella, S. V. (2008). Microchannel size effects on local flow boiling heat transfer to a dielectric fluid. *International Journal of Heat and Mass Transfer*, *51*(15-16), 3724-3735. https://doi.org/10.1016/j.ijheatmasstransfer.2008.03.013

Hedau, G., Raj, R., & Saha, S. K. (2022). Complete suppression of flow boing instability in microchannel heat sinks using a combination of inlet restrictor and flexible dampener. *International Journal of Heat and Mass Transfer*, *182*, 121937. https://doi.org/10.1016/j.ijheatmasstransfer.2021.121937

Jiang, L., Wong, M., & Zohar, Y. (2001). Forced convection boiling in a microchannel heat sink. *Journal of Microelectromechanical systems*, *10*(1), 80-87. https://doi.org/10.1109/84.911095

Kandlikar, S. G. (2004). Heat transfer mechanisms during flow boiling in microchannels. *Journal of Heat Transfer*, *126*(1), 8-16. https://doi.org/10.1115/1.1643090

Kays, W. M., & London, A. L. (1984). *Compact heat exchangers*. https://www.osti.gov/biblio/6132549

Kokate, R., & Park, C. (2024). Experimental analysis of subcooled flow boiling in a microchannel evaporator of a pumped two-phase loop. *Applied Thermal Engineering*, 123154. https://doi.org/10.1016/j.applthermaleng.2024.123154

Li, C., Fang, X., & Dai, Q. (2023). An experimental investigation of flow boiling instability of R245fa in a horizontal tube. *Physics of Fluids*, *35*(8). https://doi.org/10.1063/5.0163923

Liu, D., Lee, P. S., & Garimella, S. V. (2005). Prediction of the onset of nucleate boiling in microchannel flow. *International Journal of Heat and Mass Transfer*, *48*(25-26), 5134-5149. https://doi.org/10.1016/j.ijheatmasstransfer.2005.07.021

Markal, B., Aydin, O., & Avci, M. (2016). Effect of aspect ratio on saturated flow boiling in microchannels. *International Journal of Heat and Mass Transfer*, *93*, 130-143. https://doi.org/10.1016/j.ijheatmasstransfer.2015.10.024

Mehta, H. B., & Banerjee, J. (2014). Empirical Modeling and Experimental Investigations on Isothermal Air-Water Two-Phase Flow through Horizontal Circular Minichannel. *Journal of Applied Fluid Mechanics*, *7*(2), 227-237. https://doi.org/10.36884/jafm.7.02.19381

Priy, A., Ahmad, I., Khan, M. K., & Pathak, M. (2024). Bubble interaction and heat transfer characteristics of microchannel flow boiling with single and multiple cavities. *Journal of Thermal Science and Engineering Applications*, *16*(6), 061010. https://doi.org/10.1115/1.4065187

Raj, S., Pathak, M., & Khan, M. K. (2020). Flow boiling characteristics in different configurations of stepped microchannels. *Experimental Thermal and Fluid Science*, *119*, 110217. https://doi.org/10.1016/j.expthermflusci.2020.110217

Ramesh, B., & Gedupudi, S. (2019). On the prediction of pressure drop in subcooled flow boiling of water. *Applied Thermal Engineering*, *155*, 386-396. https://doi.org/10.1016/j.applthermaleng.2019.03.158

Saitoh, S., Daiguji, H., & Hihara, E. (2005). Effect of tube diameter on boiling heat transfer of R-134a in horizontal small-diameter tubes. *International Journal of Heat and Mass Transfer*, *48*(23-24), 4973-4984. https://doi.org/10.1016/j.ijrefrig.2017.02.012

Shah, N., Mehta, H. B., & Banerjee, J. (2024). Experimental investigations on a novel instability suppression mechanism for subcooled flow boiling in microchannel heat sink. *Applied Thermal Engineering*, *239*, 122006. https://doi.org/10.1016/j.applthermaleng.2023.122006

Singh, S. G., Kulkarni, A., Duttagupta, S. P., Puranik, B. P., & Agrawal, A. (2008). Impact of aspect ratio on flow boiling of water in rectangular microchannels. *Experimental Thermal and Fluid Science*, *33*(1), 153-160. https://doi.org/10.1016/j.expthermflusci.2008.07.014

Soupremanien, U., Le Person, S., Favre-Marinet, M., & Bultel, Y. (2011). Influence of the aspect ratio on boiling flows in rectangular mini-channels. *Experimental Thermal and Fluid Science*, *35*(5), 797-809. https://doi.org/10.1016/j.expthermflusci.2010.06.014

Sun, Y., Huang, A., Lu, J., Jiang, Y., & Wang, C. (2024). Influence of the thermophysical properties of working liquids on heat transfer performance during flow boiling in microchannels. *International Journal of Multiphase Flow*, 104856. https://doi.org/10.1016/j.ijmultiphaseflow.2024.104856

Tuckerman, D. B., & Pease, R. F. W. (1981). High-performance heat sinking for VLSI. *IEEE Electron Device Letters*, *2*(5), 126-129. https://doi.org/10.1109/EDL.1981.25367

Wang, H., Wu, S., Dai, H., Liu, X., & Zhang, C. (2023). Lattice Boltzmann investigation of flow boiling in a microchannel. *Proceedings of the Institution of Mechanical Engineers, Part C: Journal of Mechanical Engineering Science*, *237*(11), 2507-2516. https://doi.org/10.1177/0954406222108914

Wang, Y., & Sefiane, K. (2012). Effects of heat flux, vapour quality, channel hydraulic diameter on flow boiling heat transfer in variable aspect ratio micro-channels using transparent heating. *International Journal of Heat and Mass Transfer*, *55*(9-10), 2235-2243. https://doi.org/10.1016/j.ijheatmasstransfer.2012.01.044

Zhao, Q., Qiu, J., Zhou, J., Lu, M., Li, Q., & Chen, X. (2021). Visualization study of flow boiling characteristics in open microchannels with different wettability. *International Journal of Heat and Mass Transfer*, *180*, 121808. https://doi.org/10.1016/j.ijheatmasstransfer.2021.121808